

# Synthesis of $\text{LiZnBO}_3\text{:Mn}$ and Its Application to Neutron Imaging

Shunsuke Kawamata,<sup>1\*</sup> Mikio Higuchi,<sup>1</sup> Atsushi Taketani,<sup>2</sup> Tomohiro Kobayashi,<sup>2</sup>  
Yasuo Wakabayashi,<sup>2</sup> Yoshie Otake,<sup>2</sup> Kiyoharu Tadanaga,<sup>1</sup> and Junichi H. Kaneko<sup>1</sup>

<sup>1</sup>Graduate School of Engineering, Hokkaido University,  
Kita 13 Nishi 8, Kita-ku, Sapporo, Hokkaido 060-8628, Japan

<sup>2</sup>Center for Advanced Photonics, RIKEN,  
2-1 Hirosawa, Wako, Saitama 351-0198, Japan

(Received January 6, 2025; accepted March 13, 2025)

**Keywords:** neutron imaging, scintillator, translucent plate

$\text{LiZnBO}_3\text{:Mn}$  was synthesized to develop a new material for neutron imaging. Small pieces of colorless, transparent single crystals were obtained by the vertical Bridgman technique, although a large bulk single crystal was difficult to grow owing to incongruent melting and strong cleavage. Sintered compacts fired at 1000 °C showed sufficient grain growth to prepare 630  $\mu\text{m}$ -thick translucent plates. The plate emitted red light under  $\alpha$ -ray irradiation using  $^{241}\text{Am}$  as a radiation source. A neutron image showing a clear contrast of the neutron flux was obtained using a small accelerator-based neutron source.

## 1. Introduction

X-ray imaging is widely applied in security screenings to detect heavy metallic substances;<sup>(1)</sup> however, it is not easy to detect hazardous organic compounds in metallic containers.<sup>(2)</sup> In contrast, neutron beams easily penetrate metal containers, making it possible to detect substances made of light elements.<sup>(3)</sup> Neutron imaging will be used complementarily with X-ray imaging and is expected to contribute to the improvement of the accuracy of security inspections.<sup>(4)</sup> Moreover, neutron scattering by light elements such as lithium enables the visualization of the distribution of lithium concentration inside lithium-ion batteries, which has been the subject of active research in recent years.<sup>(5)</sup>

Neutrons are detected indirectly through charged particles emitted as a result of nuclear reactions between neutrons and nuclei of particular isotopes such as  $^3\text{He}$ ,  $^6\text{Li}$ , and  $^{10}\text{B}$ .  $^3\text{He}$  is widely used for neutron counting, but is unsuitable for imaging because of its gaseous state. Although imaging is being attempted using pillar-shaped gas containers, low special resolution is expected.<sup>(6)</sup> Recently, various solid neutron scintillators have been developed, such as  $\text{LiCaAlF}_6\text{:Ce}$  single crystals,<sup>(7)</sup>  $\text{LiCaAlF}_6\text{:Eu}$ ,<sup>(8)</sup> and Li-glass.<sup>(9)</sup>  $\text{LiF/ZnS:Ag}$  composite is currently used for neutron imaging with high light yield, but careful handling is necessary since the composite is made by loosely binding the two types of powder together using an organic

---

\*Corresponding author: e-mail: [kawamata.shunsuke.n5@elms.hokudai.ac.jp](mailto:kawamata.shunsuke.n5@elms.hokudai.ac.jp)  
<https://doi.org/10.18494/SAM5524>

binder.<sup>(10)</sup> The development of large, easily handled solid scintillators is a critical challenge to be addressed for neutron imaging.

In this study, we focused on  $\text{LiZnBO}_3\text{:Mn}$  as a new material for neutron imaging. Wang *et al.* reported that  $\text{LiZnBO}_3\text{:Mn}$  showed a strong fluorescence of red light upon ultraviolet and visible light excitation.<sup>(11)</sup> Since  $\text{LiZnBO}_3\text{:Mn}$  contains Li and B as the main constituents, it may be a potential target of neutron detection. Since this material is composed of relatively light elements, low sensitivity to gamma rays, which cause noise, is also expected. Its crystal structure is composed of planar triangular  $\text{BO}_3$  and tetrahedral  $\text{ZnO}_4$  units in a monoclinic unit cell with the space group  $C2/c$ .<sup>(12)</sup> The band gap of  $\text{LiZnBO}_3$  was reported as 5.57 eV.<sup>(13)</sup> As the luminescent center,  $\text{Mn}^{2+}$  substitutes the  $\text{Zn}^{2+}$  site. Although the d–d transition in  $\text{Mn}^{2+}$  is spin-forbidden,  $\text{LiZnBO}_3\text{:Mn}$  exhibits strong luminescence because  $\text{Mn}^{2+}$  occupies the center of the tetrahedron, and the transition is consequently not subject to the Laporte forbidden rule. What is needed for imaging is strong emission, and the relatively long fluorescence decay times of d–d transition are not a problem. As for the melting behavior of  $\text{LiZnBO}_3$ , there are two conflicting reports: congruent melting at 1105 °C has been reported by Buludov *et al.* in the phase diagram of the  $\text{LiBO}_2\text{–ZnO}$  system,<sup>(14)</sup> whereas Lehmann and Schadow reported that  $\text{LiZnBO}_3$  melts incongruently.<sup>(15)</sup> If  $\text{LiZnBO}_3$  melts congruently, the growth of a large bulk single crystals would be possible.

This paper deals with the crystal growth of  $\text{LiZnBO}_3\text{:Mn}$  by the vertical Bridgman (VB) method and sintering of this material to fabricate thin to translucent plates for application to neutron imaging.

## 2. Crystal Growth

The starting materials were powders of  $\text{Li}_2\text{B}_4\text{O}_7$  (98.0%),  $\text{Li}_2\text{CO}_3$  (99.99%),  $\text{ZnO}$  (99.99%), and  $\text{MnCO}_3$  (99.9%). To suppress the oxidation of  $\text{Mn}^{2+}$  to a higher valence state, a reducing atmosphere is necessary; however, the preparation of  $\text{LiZnBO}_3\text{:Mn}$  directly using the above-mentioned powders in a reducing atmosphere resulted in Zn-poor products since  $\text{ZnO}$  is reduced to Zn, which is volatile. To solve this problem,  $\text{LiZnBO}_3$  and  $\text{LiMnBO}_3$  were prepared separately in air and in a reducing atmosphere, and then they were mixed in the desired composition.  $\text{LiZnBO}_3$  was synthesized by firing the stoichiometrically mixed powders at 950 °C for 10 h in air, whereas  $\text{LiMnBO}_3$  was synthesized at 750 °C for 18 h in a reducing atmosphere of  $\text{N}_2$  with a carbon plate. The synthesized  $\text{LiZnBO}_3$  and  $\text{LiMnBO}_3$  were mixed in an agate mortar with ethanol to a composition of  $\text{LiZn}_{0.99}\text{Mn}_{0.01}\text{BO}_3$ . Crystals were grown by the VB method using a Pt crucible in air. The growth rate was 10 mm/h. The grown crystals were annealed at 900 °C for 10 h in the same reducing atmosphere as used for  $\text{LiMnBO}_3$  preparation.

Single crystals were obtained by the VB method, as shown in Fig. 1. They were colorless and transparent, but the crystal size was limited to a maximum of about 5 mm. The growth of a large bulk single crystal by the VB method is difficult for the following reasons:  $\text{LiZnBO}_3$  easily cleaves on the (002) plane because of its layered structure. Even if a large single crystal is grown, it undergoes strong thermal stresses caused by the difference in thermal expansion

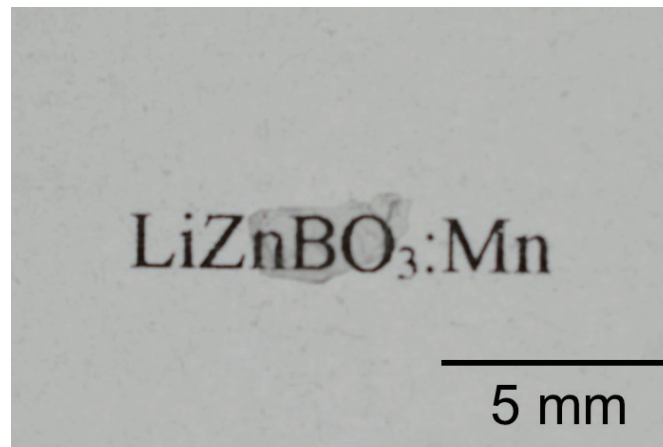


Fig. 1. (Color online) Single crystal obtained by the VB method.

coefficient between the Pt crucible and  $\text{LiZnBO}_3$ . Figure 2 shows the X-ray diffraction (XRD) pattern of the initial solidified part in crystal growth before annealing. The existence of an appreciable amount of the ZnO phase is recognized, although the main phase is  $\text{LiZnBO}_3$ . An extreme 002 peak of  $\text{LiZnBO}_3$  was observed owing to the orientation of the cleavage plane. This result indicates that  $\text{LiZnBO}_3$  melts incongruently to produce a solid ZnO phase and a liquid phase, as reported by Lehmann and Schadow.<sup>(15)</sup> Since the growth of a large bulk single crystal of  $\text{LiZnBO}_3\text{:Mn}$  by the VB method was found to be difficult, polycrystalline  $\text{LiZnBO}_3\text{:Mn}$  was prepared as discussed in the following section.

### 3. Sintering of $\text{LiZnBO}_3\text{:Mn}$

The powder for sintering was prepared by the same procedure as for crystal growth. The powder was pressed under a uniaxial pressure of 10 MPa to form a cylindrical pellet. Sintering was carried out at 900–1000 °C for 10 h in a reducing atmosphere, which is the same as for the synthesis of  $\text{LiMnBO}_3$ .

Figure 3 shows microstructures of the sintered compacts observed by scanning electron microscopy (SEM). The average grain size increased with sintering temperature, accompanied by an increase in the amount of the grain boundary phase. Since the XRD patterns of the sintered compacts in Fig. 4 proved the existence of a small amount of the  $\text{LiBO}_2$  phase, the grain boundary phase is expected to be  $\text{LiBO}_2$ . Some of the zinc constituent may be reduced to metallic zinc and sublimated owing to the reducing atmosphere during sintering, resulting in the formation of  $\text{LiBO}_2$ . The formation of the  $\text{LiBO}_2$  phase is favorable for obtaining dense sintered compacts, because it forms a liquid phase, through which mass diffusion is promoted. A higher sintering temperature above 1000 °C was unfavorable since the softening of the pellets occurred because of an excessive amount of the  $\text{LiBO}_2$  phase. Regardless of the sintering temperature and grain size, parallel lines are observed within the grains, which are expected to be due to cleavage.

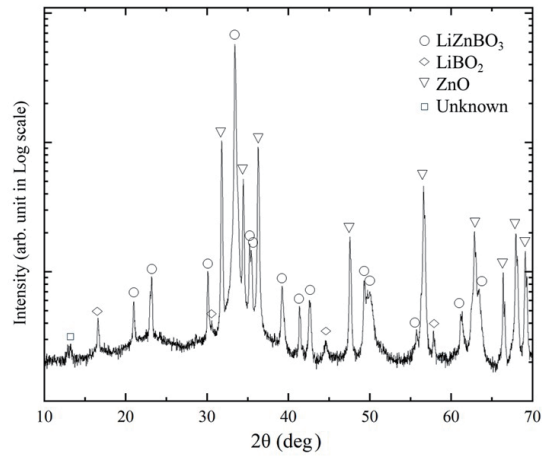


Fig. 2. XRD pattern of the initial solidified part of the crystal grown by the VB method.

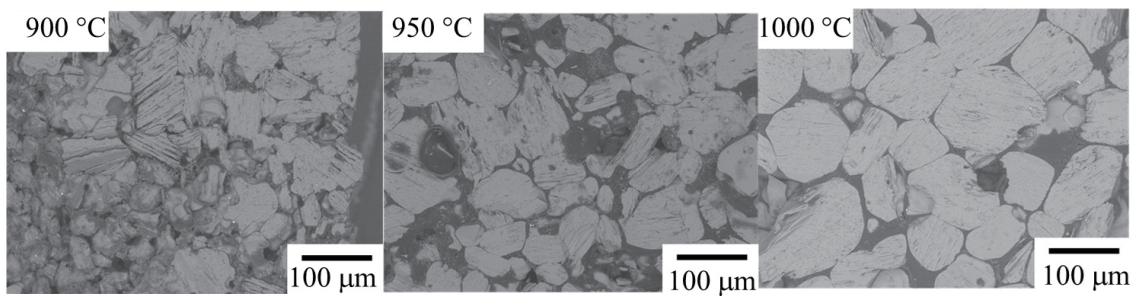


Fig. 3. Microstructures of the sintered compacts fired at 900, 950, and 1000 °C.

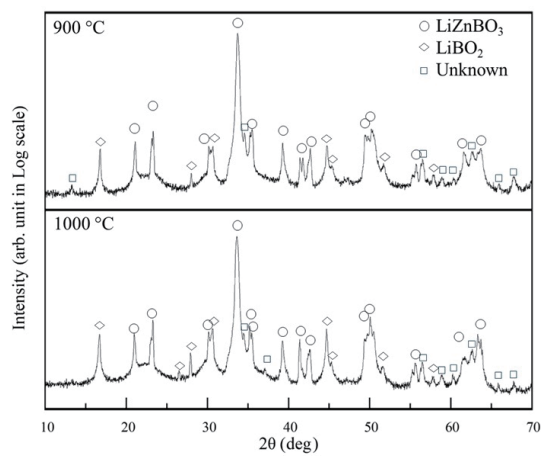


Fig. 4. XRD patterns of the sintered compacts fired at 900 and 1000 °C.

The sintered compacts showed intense red fluorescence, as shown in Fig. 5. These excitation and emission spectra were similar to those reported by Wang *et al.*<sup>(11)</sup> The broad emission band from 500 to 800 nm by d–d transition is suitable for observation with a CCD camera, which was used to detect the scintillation light as described below.

#### 4. Scintillation Properties

To investigate the scintillation properties of the  $\text{LiZnBO}_3\text{:Mn}$  sintered compacts, thin plates were fabricated as follows, using the cylindrical sintered compacts described in the previous section and additional sintered compacts produced by cold isostatic pressing for large-area imaging. Sintered compacts were impregnated with epoxy resin for 3 days, and then one side of the compacts was ground with abrasive paper to make it flat. After bonding the ground surface to a glass substrate with epoxy resin, the compacts were again ground down to 180 or 630  $\mu\text{m}$  with abrasive paper. After grinding, the thin plate was translucent despite its thickness being 630  $\mu\text{m}$ , as shown in Fig. 6. These thin plates were used to evaluate the scintillation properties.

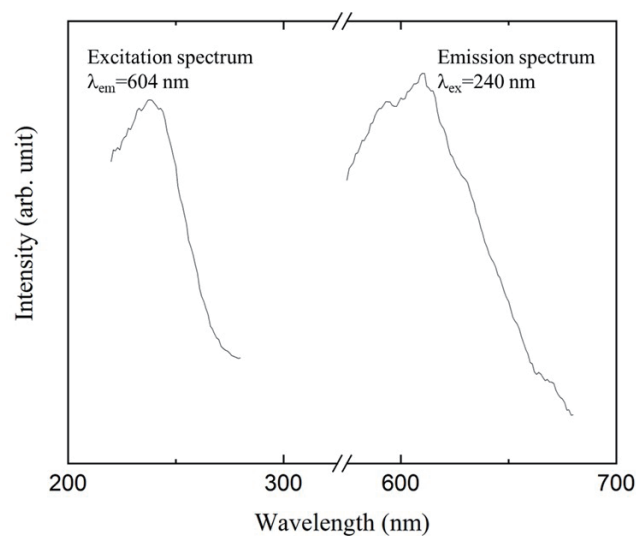


Fig. 5. Excitation and emission spectra of the sintered compact of  $\text{LiZnBO}_3\text{:Mn}$ .

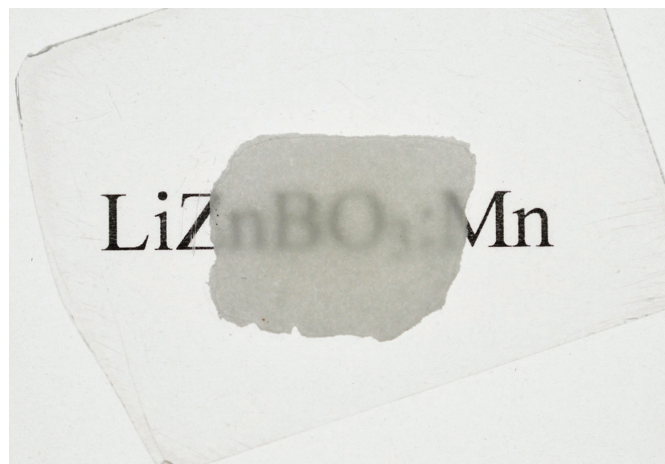


Fig. 6. (Color online) Translucent plate of  $\text{LiZnBO}_3\text{:Mn}$  with a thickness of 630  $\mu\text{m}$ .

Since the nuclear reactions of neutrons with Li and B result in the production of  $\alpha$ -rays in both cases, it is important to investigate whether  $\text{LiZnBO}_3\text{:Mn}$  will undergo scintillation upon irradiation with an  $\alpha$ -ray. A thin plate of 160  $\mu\text{m}$  thickness was irradiated with an  $\alpha$ -ray from  $^{241}\text{Am}$  ( $5.6 \times 10^3 \text{ Bq}$ ) in a dark room using a single-lens reflex camera (Nikon D3200), as shown in Figs. 7(a) and 7(b). Figure 7(c) shows the scintillation of the  $\text{LiZnBO}_3\text{:Mn}$  thin plate. Circular-shaped red emission is observed, which matches the shape of the sample at an exposure time of 5 min, while red spots in the outer region are noise. Thus, the  $\text{LiZnBO}_3\text{:Mn}$  thin plate is expected to be used for neutron imaging.

Neutron imaging experiments were carried out using a RIKEN accelerator-driven compact neutron source (RANS) from which a neutron flux of  $100000 \text{ n cm}^{-2} \text{ s}^{-1}$  is generated.<sup>(16)</sup> The irradiation time was 5 min. Figure 8 shows the schematic diagram of the experimental setup for neutron imaging. A boron nitride polycrystal processed into the shape of “N” was used as an absorber to take neutron images [Fig. 9(a)]. The thickness of the absorber was 2.9 mm, which was enough to absorb most of the thermal neutron flux irradiated onto it. The  $\text{LiZnBO}_3\text{:Mn}$  thin plate and the absorber were attached to both sides of an aluminum plate with polyimide tape [Fig. 9(b)]. The neutron flux was irradiated for 5 min, and the neutron image was taken with a CCD camera.

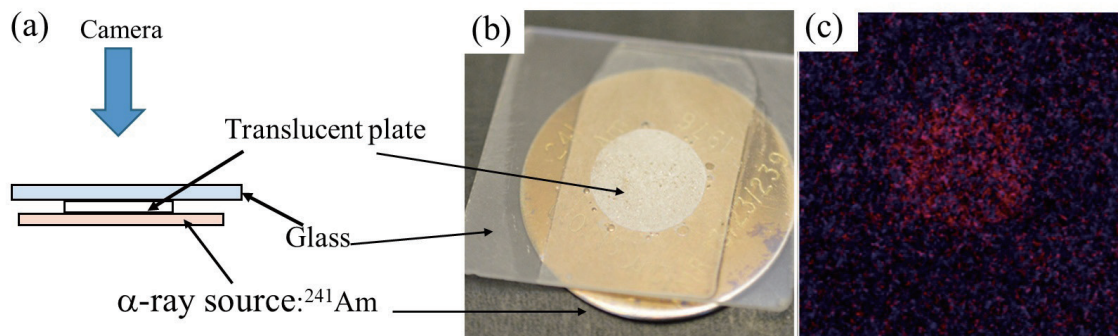


Fig. 7. (Color online) (a), (b) Setup for  $\alpha$ -particle irradiation using  $^{241}\text{Am}$  and (c)  $\alpha$ -particle scintillation of the  $\text{LiZnBO}_3\text{:Mn}$  thin plate in a dark room.

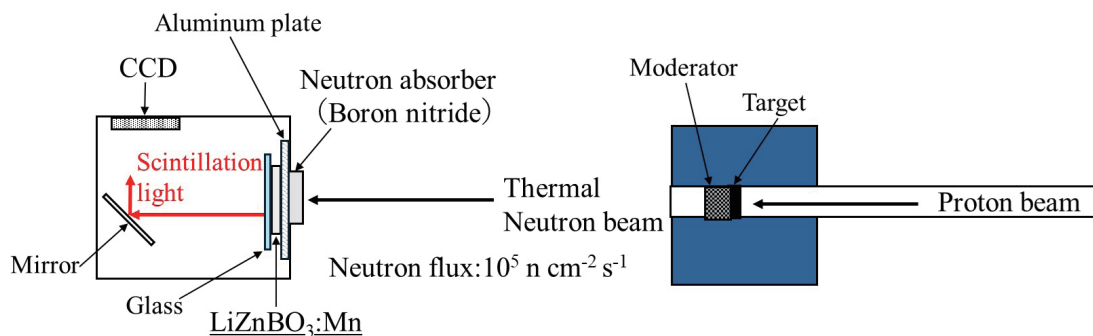


Fig. 8. (Color online) Schematic diagram of the neutron imaging experiment using RANS.

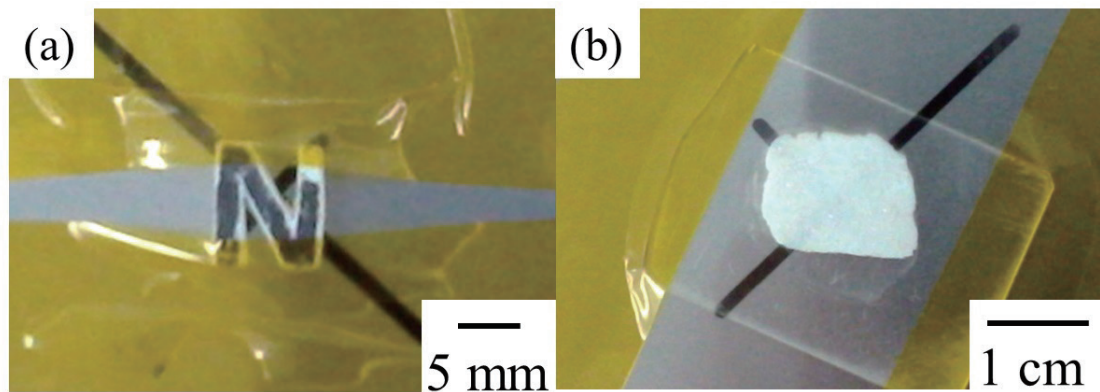


Fig. 9. (Color online) (a) Boron nitride neutron absorber. (b) LiZnBO<sub>3</sub>:Mn plate.

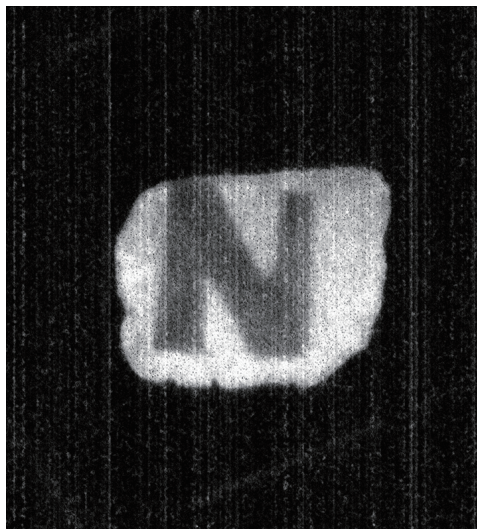


Fig. 10. Neutron image using a LiZnBO<sub>3</sub>:Mn thin plate.

A neutron image was successfully obtained, as shown in Fig. 10. Part of the neutron flux was effectively absorbed by the N-shaped boron nitride absorber, resulting in a dark image, and the area directly irradiated by the neutrons was brightened. The brightness of the LiZnBO<sub>3</sub>:Mn thin plate was 3.4% of that of <sup>6</sup>LiF/ZnS. From the thermal neutron capture cross sections of <sup>6</sup>Li and <sup>10</sup>B, the absorption of neutrons by Li and B in the 630 μm-thick LiZnBO<sub>3</sub>:Mn thin plate was calculated to be 7.1 and 55.1%, respectively, since unenriched raw materials were used in this study. Most of the neutrons are therefore absorbed by <sup>10</sup>B, from which charged particles having a relatively low total energy of 2.8 MeV compared with those of <sup>6</sup>Li (4.8 MeV) are generated.<sup>(17)</sup> If <sup>6</sup>Li- and <sup>11</sup>B-enriched raw materials are used to synthesize LiZnBO<sub>3</sub>:Mn, neutrons are absorbed only by <sup>6</sup>Li, which produces charged particles of high energy, and a significant improvement in light yield is expected.

## 4. Conclusions

We focused on LiZnBO<sub>3</sub>:Mn showing strong red fluorescence as a new material for neutron imaging. The growth of a large bulk single crystal of LiZnBO<sub>3</sub>:Mn was difficult owing to strong cleavage and incongruent melting. Using a polycrystalline thin plate, a neutron image was successfully obtained and the brightness was 3.4% of that of LiF/ZnS. Since the use of <sup>6</sup>Li- and <sup>11</sup>B-enriched raw materials is expected to significantly improve the light yield, LiZnBO<sub>3</sub>:Mn polycrystalline thin plates are a promising material for neutron imaging.

## References

- 1 D. Saavedra, S. Banerjee, and D. Mery: *Neural Comput. Appl.* **33** (2021) 7803. <https://doi.org/10.1007/s00521-020-05521-2>
- 2 S. Huang, X. Wang, Y. Chen, J. Xu, T. Tang, and B. Mu: *Opt. Express* **27** (2019) 337. <https://doi.org/10.1364/OE.27.000337>
- 3 A. X. da Silva and V. R. Crispim: *Radiat. Phys. Chem.* **61** (2001) 767. [https://doi.org/10.1016/S0969-806X\(01\)00399-1](https://doi.org/10.1016/S0969-806X(01)00399-1)
- 4 R. C. Runkle, T. A. White, E. A. Miller, J. A. Caggiano, and B. A. Collins: *Nucl. Instrum. Methods Phys. Res. A* **603** (2009) 510. <https://doi.org/10.1016/j.nima.2009.02.015>
- 5 D. Gupta, Y. Zhang, Z. Nie, and G. M. Koenig Jr.: *J. Ind. Eng. Chem.* **133** (2024) 219. <https://doi.org/10.1016/j.jiec.2023.11.060>
- 6 K. Fujita, H. Takahashi, P. Siritiprussamee, H. Niko, K. Nishi, Y. Takada, T. Oku, J. Suzuki, T. Ino, H. M. Shimizu, and M. Furusaka: *Nucl. Instrum. Methods Phys. Res. A* **580** (2007) 1027. <https://doi.org/10.1016/j.nima.2007.06.057>
- 7 J. Iwanowska, L. Swiderski, M. Moszynski, T. Yanagida, Y. Yokota, A. Yoshikawa, K. Fukuda, N. Kawaguchi, and S. Ishizu: *Nucl. Instrum. Methods Phys. Res. A* **652** (2011) 319. <https://doi.org/10.1016/j.nima.2010.09.182>
- 8 N. V. Shiran, A. V. Gektin, S. V. Neicheva, V.A. Kornienko, K. Shimamura, and N. Ishinose: *J. Lumin.* **102–103** (2003) 815. [https://doi.org/10.1016/S0022-2313\(02\)00647-6](https://doi.org/10.1016/S0022-2313(02)00647-6)
- 9 M. Koshimizu, K. Iwamatsu, M. Taguchi, S. Kurashima, A. Kimura, T. Yanagida, Y. Fujimoto, K. Watanabe, and K. Asai: *J. Lumin.* **169** (2016) 678. <https://doi.org/10.1016/j.jlumin.2015.04.015>
- 10 A. Osovizky, K. Pritchard, J. Ziegler, E. Binkley, Y. Yehuda-Zada, and P. Tsai: *IEEE Trans. Nucl. Sci.* **65** (2018) 1025. <https://doi.org/10.1109/TNS.2018.2809567>
- 11 H. Wang, L. Wu, H. Yi, B. Wang, L. Wu, Y. Gua, and Y. Zhang: *Dalton Trans.* **44** (2015) 1427. <https://doi.org/10.1039/C4DT02626H>
- 12 X. Chen, C. Yang, X. Chang, H. Zang, and W. Xiao: *Solid State Sci.* **11** (2009) 2086. <https://doi.org/10.1016/j.solidstatesciences.2009.08.024>
- 13 V. Ragupathi, S. Krishnaswamy, P. Panigrahi, and G. S. Nagarajan: *Mater. Sci. Energy Technol.* **2** (2019) 267. <https://doi.org/10.1016/j.mset.2018.12.003>
- 14 N. T. Buludov, Z. S. H. Karaev, and G. K. Abdullaev: *Russ. J. Inorg. Chem.* **31** (1986) 1215.
- 15 H. A. Lehmann and H. Schadow: *Z. Anorg. Allg. Chem.* **348** (1966) 42. <https://doi.org/10.1002/zaac.19663480106>
- 16 Y. Otake: *Rev. Laser Eng.* **46** (2018) 654. [https://doi.org/10.2184/lsej.46.11\\_654](https://doi.org/10.2184/lsej.46.11_654)
- 17 A. J. Deruytter and P. Pelfer: *J. Nucl. Energy* **21** (1967) 833. [https://doi.org/10.1016/0022-3107\(67\)90094-9](https://doi.org/10.1016/0022-3107(67)90094-9)